VORTEX STRUCTURE IN THE SCOUR HOLE BY GATE OPENING OF HYDRAULIC STRUCTURE

Jin Hong Kim[1], and Jae Wan Choe[2]

1. Department of Civil Engineering, Chung-Ang University, Gyunggi-Do, Korea
2. Division of Civil and Environment Engineering, Kwangju University, Kwangju, Korea

Abstract: Jet flow can occur by gate opening at downstream of a hydraulic structure such as weir or drainage gate. If the stream bed is not hard or the bed protection is not sufficient, vortex erosion occurs and a resulting scour hole will be formed due to the high shear stress of the jet flow. Once the scour hole is formed, a vortex occurs in it and this vortex causes additional erosion. If this erosion continues and reaches to the hydraulic structure, it can undermine the bottom of the hydraulic structure and this will lead to failure of the structure itself. Thus, it is necessary to define the physical features of the vortex structure in the scour hole for the design of the bed protection. This study presents the turbulent vortex structure in the scour hole by the gate opening of the hydraulic structure. Characteristics of vortex motion, circulation, vortex scale and vortex velocity were analyzed through experiments. Experimental results of the vortex velocity were compared with theoretical ones. From these, circulation and vortex scale were obtained with known values of inflow depth, inflow velocity and scale of scour hole

Key Words jet flow, vortex erosion, scour hole, vortex structure, circulation, vortex scale

1. INTRODUCTION

Localized scour at the outlet of the hydraulic structures such as weirs, sluice gates and low dams can cause dangerous erosion problems. Jet flow, which occurs by the gate opening of such structures due to flood or artificial sediment flushing, has a considerable potential for scour (Miwa, 1990). Sheet erosion occurs which is characterized by the removal of a layer with a certain thickness of the bottom surface (Kim and Kim, 1999), and the resulting scour hole is formed at the outlet of the hydraulic structure due to the high shear stress of the jet flow. This erosion proceeds to the downward direction. It is called the primary erosion.

Once the scour hole is formed, a vortex occurs in it and this vortex causes additional erosion. It is called the secondary erosion. The secondary erosion occurs by the line vortex and it proceeds to the upward direction. The line vortex means that it has the same size and the same strength to the transverse direction. Vortex erosion occurs at the upstream part of bottom surface hole which is characterized by the entrainment of bottom sediments, and its quantity is not so large compared with the primary erosion.

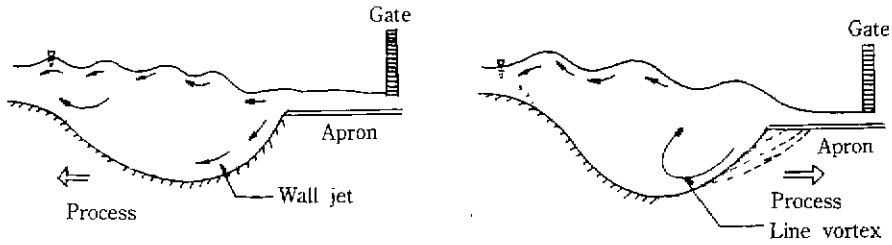

(a) Primary Erosion (b) Secondary Erosion

Fig. 1. Physical Features of Primary and Secondary Erosion

Table 1. Comparison between Primary and Secondary Erosion

	Primary erosion	Secondary erosion
Mechanism	Jet flow	Line vortex
Characteristics	Sheet erosion	Vortex erosion
Direction	Downward	Upward
Quantity	Large	Small
Intensity	Strong	Strong

Fig. 1 shows the physical features of the primary and the secondary erosion, and the difference between them is summarized in Table 1.

The vortex structure which occurs during the process of the secondary erosion must be considered for the design of the bed protection, since it proceeds to the upward direction. If the secondary erosion continues and reaches to the hydraulic structure, it can undermine the bottom of the hydraulic structure.

Fig. 2 shows the structure of a line vortex and the resulting scour hole downstream of a weir by gate opening. Here the line vortex means that it has the same size and the same strength to the transverse direction. The line vortex lifts sediment particles since the upward momentum of the vortex is larger than the gravity force of the sediment particle, which supports the existing concept that the local concentration of a suspended sediment is related to the intensity of the vertical component of the turbulent vortices (Ikeda and Asaeda 1983). The macroturbulence of the line vortex consists of a continuous and strong upward flow compared with turbulence formed at the lee-side of a sand ripple in the river whose upward flow is not so strong and intermittent. In Fig. 2(a), the line vortex causes an additional scour by the three failure mechanism, i.e., slip circle, liquefaction and internal erosion, and finally will lead to the deformation of the structure itself as shown in Fig. 2(b). The main

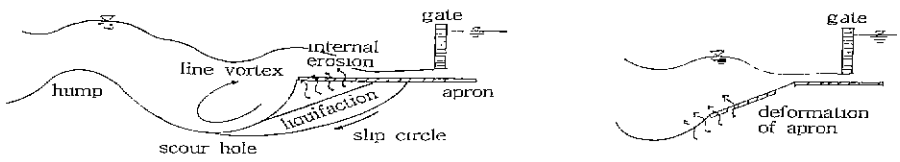

(a) Line Vortex (b) Deformation of Structure

Fig. 2. Structure of Line Vortex and Scour Hole

purpose of this study is to define the physical features of the turbulent vortex structure in the scour hole through experiments and computational procedures.

2. EXPERIMENTAL APPARATUS AND PROCEDURE

Experiment was done in a recirculating channel of 0.4m and 10m long. Artificial bed was made to simulate the actual profile of the scour hole using a cement mortar. Hydraulic conditions of this artificial bed profile were essentially the same as those of the sand bed profile for the movable bed conditions. Velocity field of the line vortex in a scour hole was measured using aluminum particles and a motor driven camera. As a tracer method, aluminum particles mixed with a neutral detergent were put into the channel at the upstream end. Photos were taken using a motor driven camera with the vertical light sheet by a slide projector in dark condition. Then, the velocity could be measured from the length of a trajectory of aluminum particle divided by exposure time. A slit width of the slide projector and exposure time of the camera were adjusted considering concentration and velocity of the aluminum particles. By a trial and error, 0.5~0.7mm of the slit width and 1/15~1/30 second of the exposure time were suitable values. Experimental conditions are shown in Table 1. Here, h_0 is an entering flow depth into the scour hole, u_0 is the mean velocity of the entering flow, I_b is the slope of an artificial bed and T is an exposure time of the motor driven camera. the type 1 and the type 2 of the artificial bed correspond to those of the instantaneous sand bed profile when the large macroturbulence occurred at a movable bed

Table 2. Summary of Experimental Conditions

Run no.	h_0 (cm)	u_0 (cm/s)	I_b (-)	T (s)	Remark
R1	0.5	75	0.40	1/15	type 1
R2	0.7	105	0.40	1/15	type 1
R3	1.0	120	0.40	1/15	type 1
R4	1.2	132	0.40	1/15	type 1
R5	1.5	145	0.40	1/30	type 1
R6	2.0	154	0.40	1/30	type 1
R7	0.5	81	0.45	1/15	type 2
R8	1.0	122	0.45	1/15	type 2

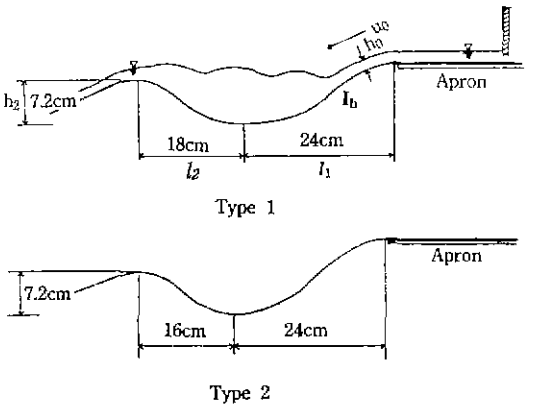

Fig. 3. Rigid Bed Model for Scour Hole

experiment. They are also shown in Fig. 3.

Photo development was done under the condition of ISO up to 3200 in order to obtain clear trajectory in pictures taken in dark condition. This photo was used for obtaining a digitized velocity vector, contour map of a velocity and a vorticity. Figs. 4 and 5 show this procedure.

3. EXPERIMENTAL RESULTS

3.1 Vortex and Flow Features in Scour Hole

Fig. 6 shows the time variation of streamlines of the vortex motion for R1 case of Table 1. Here T_* is a dimensionless time;

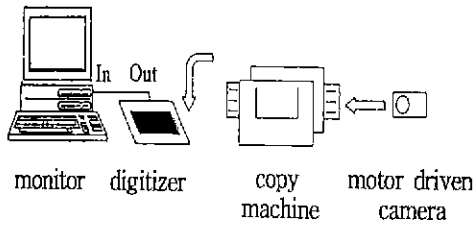

Fig. 4. Data System for Flow Trajectory

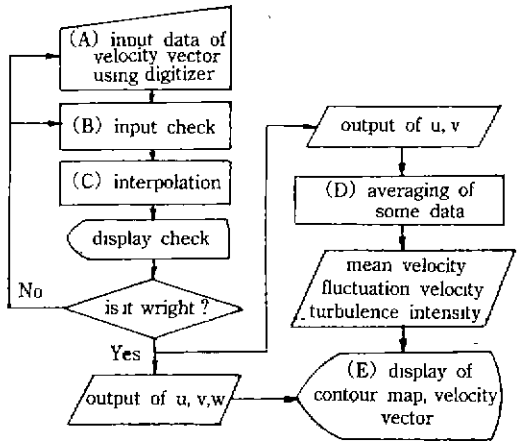

Fig. 5. Flow Chart for Data System

$$T_* = t / T \qquad (1)$$

where, T is a period of one cycle of the vortex motion and t is a time corresponding to instantaneous stage of the vortex motion.

An outer large vortex occurs covering the whole section of the scour hole, and one or two inner vortices occur inside the outer vortex. The inner vortex forms an inclined eye-shaped one initially as is shown in (1) of Fig. 6. Then, this vortex is divided into two horizontal eye-shaped vortices which have an equal sinks shown in (2) of Fig. 6. These vortices become apart and one of them becomes smaller finally disappeared as shown in (3), (4) and (5) of Fig. 6. Time variation of the vortex motion for other cases in Table 1 was almost the same as for R1 case.

Fig. 7 shows a vortex motion in the scour hole. An entering velocity becomes accelerated from a crest to a through but becomes decelerated changing a vertical

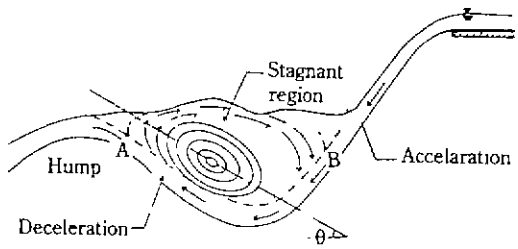

A : separation point
B : reattachment point

Fig. 7. Vortex Motion in Scour Hole

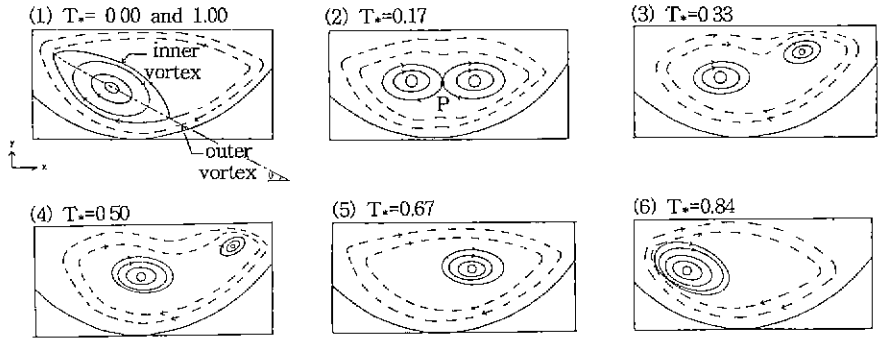

Fig. 6. Schematic Diagram of Vortex Motion (R1 Case)

direction from the through to the crest of a downstream hump. Separation occurs at the trailing edge of a scour hole and reattachment occurs at the acceleration part. These separation of the flow over a trailing edge and a subsequent reattachment lead to an outer large vortex. Also, the inner inclined eye-shaped vortex occurs at the trailing part of the scour hole within the outer vortex. This vortex is thought to be formed due to the concentration of a vorticity which was supplied from the separation point. The axis of an inner vortex is almost parallel to the slope of downstream hump.

3.2 Physical Phenomenon of Circulation

Fig. 8 shows the time variation of the circulation of the line vortex. The circulation fluctuates with time, which is almost the same phenomenon in all the cases irrespective of the bed type and discharge. Here the following results are extracted. Circulation takes its maximum value where the inner vortex locates along the slope of a downstream hump as shown in (1) of Fig. 6, but takes its minimum value when the inner vortex is divided into the equal vortices as shown in (2) of Fig. 6. Two horizontal inner vortices form a saddle point P, and with this effect the strength of two vortices become counter-balanced and the circulation becomes minimized. When the two vortices become apart, one recovers its circulation energy and the total circulation also recovers its energy compared with that observed in (2) of Fig. 6.

Fig. 9 shows the dimensionless distribution of circulation for R1 case as a function of the dimensionless vortex length. Here Γ_m means the maximum circulation and L_m is the maximum vortex length. Circulation Γ is calculated from the corresponding vortex length L. In Fig. 9, Tanaka(1986)'s data which were obtained from the experiments of flow over rippled model are also included. Here case 1 to case 6 was categorized according to the bed profile. It can be seen that the circulation increases linearly in proportion to the vortex length irrespective of the bed profile and the vortex structure.

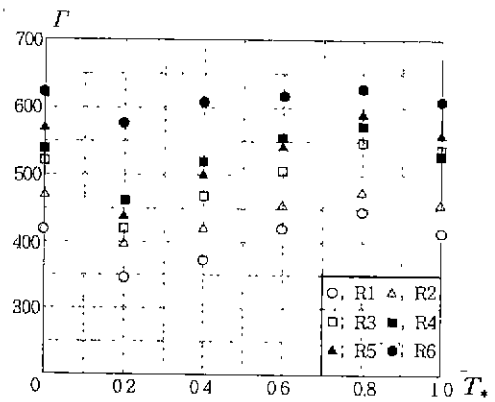

Fig. 8. Time Variation of Circulation of Line Vortex

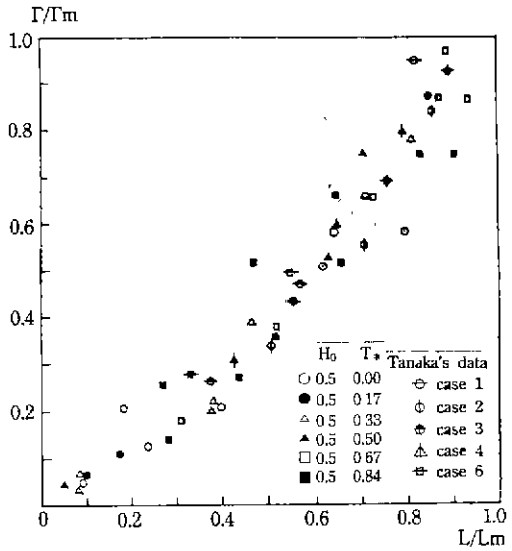

Fig. 9. Dimensionless Distribution of Circulation

3.3 Estimation of Circulation and Vortex Scale Using Outer Parameters

Circulation can be expressed as follows using the relevant outer parameters,

$$\Gamma = k \times L u_0 \tag{2}$$

where, L is the length between the crests which is sum of l_1 and l_2 shown in Fig. 3, u_0 is also shown in Fig. 3 and k is constant. Experimental results are shown in Fig. 10. It can be seen that k is almost equal to 0.12 irrespective of the Reynolds number, and the circulation can be roughly estimated with known values of L and u_0.

Fig. 11 shows the relationship between the scale of an inner vortex and the hump height. Here, l_x and l_y are the horizontal and the vertical scale of the inner vortex, respectively and h_2 is the height of a downstream hump shown in Fig. 3. As can be seen in Fig. 3, the vertical scale of the inner vortex is almost equal to the hump height and the horizontal scale is equal to 1.4~1.8 times of the hump height. These results were nearly the same as Tanaka (1986)'s experimental ones. While, the horizontal scale L_x and the vertical scale L_y of the outer vortex are almost equal to the length between the crests L and the hump height h_2, respectively. This is due to the fact that the outer vortex consists of the separation and the reattachment point of the flow, and hence it is formed throughout the whole section of the scour hole as shown in Fig. 7.

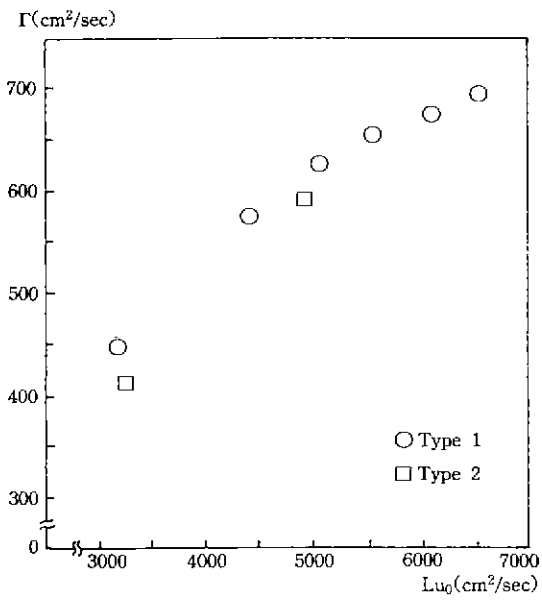

Fig. 10. Relation Between Circulation and Outer Parameter

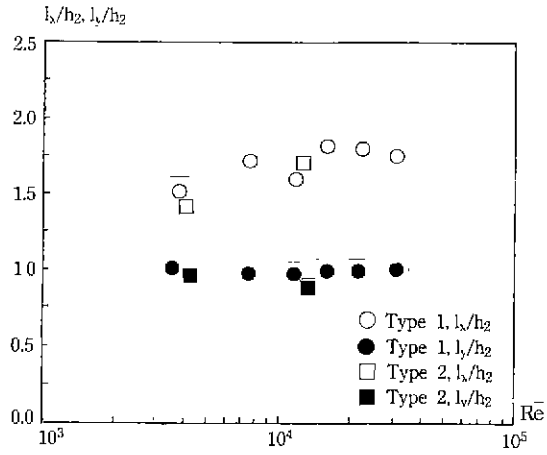

Fig. 11. Dimensionless Vortex Scale as a Function of Reynolds Number

4. THEORETICAL APPROACH FOR VORTEX VELOCITY

As was seen in (1) of Fig. 6, the inner vortex forms the inclined eye-shaped one, which can be analyzed as follows.

The complex potential for a series of $2n+1$ vortices of the same strength Γ spaced along the x-axis at the distance a part with the center one at the origin is (Milne-Thompson, 1968),

$$W(z)=-\frac{i\Gamma}{2\pi}\ln\frac{\pi z}{a}(1-\frac{z^2}{a^2})(1-\frac{z^2}{4a^2})\cdot\cdots\cdot(1-\frac{z^2}{n^2a^2})+const \tag{3}$$

when $n\to\infty$, this may be written

$$W(z)=-\frac{i\Gamma}{2\pi}\ln(\sin\frac{\pi z}{a})=\frac{\Gamma}{2\pi i}\ln(\sin\frac{\pi z}{a}) \tag{4}$$

Since the inner vortex forms the inclined eye-shaped one whose axis making an angle θ with the x-axis, eq. (4) becomes as;

$$\begin{aligned}W(z) &= \frac{\Gamma}{2\pi i}\ln(\sin\frac{\pi}{a}z)\,e^{-i\theta}\\ &= \frac{\Gamma}{2\pi i}\ln(\sin\frac{\pi}{a}z)(\cos\theta-i\sin\theta)\end{aligned} \tag{5}$$

$$\begin{aligned}\frac{dW(z)}{dz} &= -\frac{\Gamma}{2a}(\sin\theta+i\cos\theta)\cot\frac{\pi z}{a},\quad z=x+yi\\ &= \frac{-\Gamma}{2a}(\sin\theta+i\cos\theta)(\frac{\sin\frac{2}{a}\pi x-i\sinh\frac{2}{a}\pi y}{\cosh\frac{2}{a}\pi y-\cos\frac{2}{a}\pi x})\\ &= -(u-iv)\end{aligned} \tag{6}$$

Separating into real and imaginary parts, the horizontal and the vertical velocity of the vortex becomes as;

$$u=\frac{\Gamma}{2a}\frac{\sin\theta\sin\frac{2}{a}\pi x+\cos\theta\sinh\frac{2}{a}\pi y}{\cosh\frac{2}{a}\pi y-\cos\frac{2}{a}\pi x} \tag{7}$$

$$v=-\frac{\Gamma}{2a}\frac{\cos\theta\sin\frac{2}{a}\pi x-\sin\theta\sinh\frac{2}{a}\pi y}{\cosh\frac{2}{a}\pi y-\cos\frac{2}{a}\pi x} \tag{8}$$

Comparisons of the velocities between the calculational and the experimental results are shown in Fig. 12. Here, $\theta=0$ and $\theta=21.8$ correspond to the horizontal and the inclined inner vortex whose angle is equal to the slope of the hump shown in (1) of Fig. 6, respectively. Parameters shown in Fig. 12 are;

$$x_*=\frac{x}{a},\quad y_*=\frac{y}{a},\quad u_*=\frac{u}{(\Gamma/2a)},\quad v_*=\frac{v}{(\Gamma/2a)} \tag{9}$$

In Fig. 12, the origin (0,0) becomes a singular point where the horizontal and vertical velocity becomes infinite. Theoretical value for vorticity Ψ in the origin is calculated as;

$$\Psi = \frac{\partial v}{\partial x}-\frac{\partial u}{\partial y}=0 \tag{10}$$

Flow becomes irrotational but the circulation around the origin is not zero since the highly concentrated vorticity, i. e., vortex filament exists at the origin. In (3), (4) of Fig. 12, points $(\pm0.5,0)$ are saddle and the vertical velocity becomes zero. Theoretical values of u and v become infinite at the origin with the effect of a vortex filament. But the experimental value approaches zero towards the origin supporting the concept of Rankine's combined vortex, velocity profile of which is represented by the following equations.

$$\begin{aligned}v' &= \frac{x}{x_0}v,\quad(-x_0\le x\le x_0)\\ v' &= v,\quad(x>x_0, x<-x_0)\end{aligned} \tag{11}$$

$$\begin{aligned}u' &= \frac{y}{y_0}u,\quad(-y_0\le y\le y_0)\\ u' &= u,\quad(y>y_0, y<-y_0)\end{aligned} \tag{12}$$

The values of x_0 and y_0 are found to be approximately $0.25a$ and $0.50a$, respectively through the experiments.

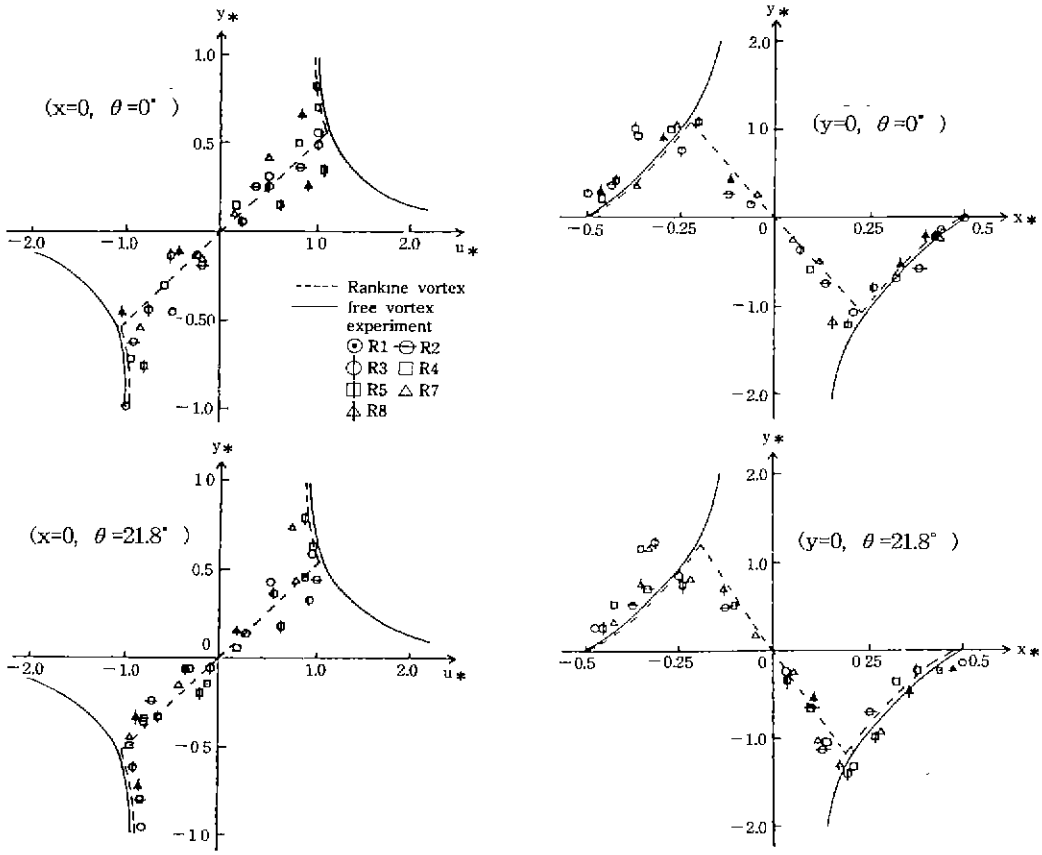

Fig. 12. Comparisons of u_* and v_* between Calculational and Experimental Results

5. PROBABILITY DENSITY DISTRIBUTION FOR VERTICAL VELOCITY OF TURBULENT VORTICES

It is well known that the sand particles are entrained into the water from the trailing edge of the scour hole by the vertical component of the turbulent vortices (Asaeda et al., 1989). The commencement of the sand particle is caused by the vertical velocity fluctuation near the surface of the sand bed. To obtain the initial velocity of the sand particle, it is necessary to determine the vertical velocity of the turbulent vortices.

The magnitude of the vertical fluid velocity fluctuates and follows the normal distribution with a mean $\bar{v}$ and a standard deviation v_{*1} near the rippled sand bed. Thus, the probability density function is given by (Asaeda et al., 1989),

$$f(v) = \frac{1}{\sqrt{2\pi}\, v_{*1}} \exp\left[-\frac{1}{2}\left(\frac{v-\bar{v}}{v_{*1}}\right)^2\right] \qquad (13)$$

Here, v_{*1} is also known to be the local friction velocity at the trailing edge of the scour hole (Asaeda et al., 1989). It can be estimated that the probability density distribution for the vertical velocity of the turbulent vortices in the scour hole also follows the same normal distribution as eq.

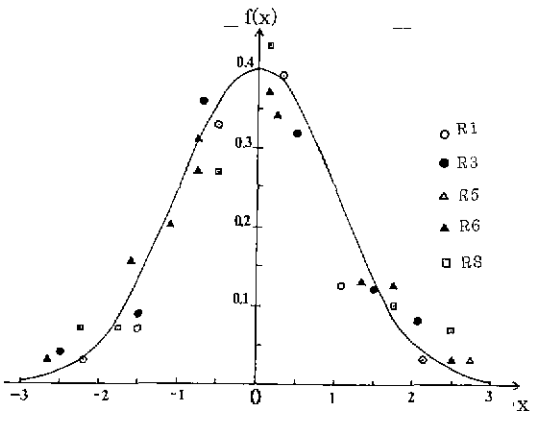

Fig. 13. Probability Density Distribution for Vertical Velocity of Turbulent Vortices

(13), since the characteristics of the vortex circulation and the vortex scale are almost the same as those of Tanaka (1986)'s experiments in the rippled model as was explained in 3.2 and 3.3.

If the standardized variable x is used instead of v, the eq. (13) becomes as;

$$f(x)=\frac{1}{\sqrt{2\pi}}\exp\left(-\frac{1}{2}x^2\right) \quad \text{where, } x=\frac{v-\bar{v}}{v_{*1}} \qquad (14)$$

following the standardized normal distribution : N(0,1).

Fig. 13 shows the comparison between the theoretical values of eq. (14) and the experimental ones.

A fairly good agreement is seen between these two values. To check the goodness of fit, χ^2-test was done. Calculated deviation $\chi_0^2=6.296$ if the significant level $\alpha=5\%$ and the interval number $k=6$. For given values of $k-1$ degree of freedom and the significant level α, the value $C=11.07$ as a solution of $P(\chi^2<C)=95\%$ from the table of χ^2 distribution is obtained. Since $\chi_0^2<C$, The hypothesis that a vertical turbulent velocity follows the normal distribution is not rejected.

6. CONCLUSION

Characteristics of the vortex motion, circulation, vortex scale and vortex velocity were analyzed through experiments. Experimental results of the vortex velocity were compared with theoretical ones. From these, following conclusions were obtained.

(1) An outer large vortex occurred covering the whole section of the scour hole, and inner vortices occurred inside the outer vortex.

(2) Circulation was increased linearly in proportion to the vortex length irrespective of the bed profile and the vortex structure.

(3) Circulation and vortex velocity were obtained with known values of the length between crests, the inflow depth and the inflow velocity.

(4) Comparisons of vortex velocity between experimental and calculational results showed good agreements if the concept of Rankine's combined vortex was used.

(5) Probability density distribution for the vertical velocity of the turbulent vortices in the scour hole followed the normal distribution.

REFERENCES

Asaeda, T., Nakai, M., Shyam, K.M., and Tamai, N. (1989). "Sediment entrainment in channel with rippled bed." *Journal of Hydraulic Engineering*, ASCE, Vol. 115, No. 3, pp. 327-339.

Ikeda, S. and Asaeda, T. (1983). "Sediment suspension with rippled bed." *Journal of Hydraulic Engineering*, ASCE, Vol. 109, No. 3, pp. 78-85.

Kim, J.H. (1992). "Characteristics of vortex

structure and its shear velocity in a scour hole." *Journal of Agricultural Engineering*, KSAE, Vol. 34, No. 1, pp. 45-59.

Kim, J.H. and Kim. J.S. (1999). "Sheet erosion in embankment of noncohesive materials due to unsteady overflow." *Journal of Civil Engineering*, KSCE, Vol. 3, No. 1, pp. 57-64.

Milne-Thompson, L.M. (1968). *Theoretical Hydrodynamics,* The Macmillan Company, New York, N.Y., pp. 172-176.

Miwa, H. (1990), "Process of flushing sands accumulated under gates on a dam by sluice outlet." *Proceedings 34th Hydraulic Conference of JSCE*, Tokyo, Japan, Vol. 1, pp. 247-252.

Tanaka, H. (1986), "On the structure of flow over rippled model." *Proceedings 30th Hydraulic Conference of JSCE*, Hirosima, Japan, Vol. 1, pp. 595-600.

Jin Hong Kim, Department of Civil Engineering, Chung-Ang University, San 40 -1, Nae-ri, Daeduck-myun, Gyunggi-Do, 456-756, Korea.
(email: jinhkim@cau.ac.kr)

Jae Wan Choe, Division of Civil and Environment Engineering, Kwangju University, 592-1 Jinwal-Dong, Nam-Gu, Kwangju, 502-703 Korea.

(Received September 3, 1999; revised October 4, 1999; accepted November 1, 1999.)